

BFKL phenomenology*

G. CHACHAMIS

Instituto de Física Teórica UAM/CSIC & Universidad Autónoma de Madrid, C/
Nicolás Cabrera 15, E-28049 Madrid, Spain

We present some of the topics covered in a series of lectures under the same title that was given at the “Summer School on High Energy Physics at the LHC: New trends in HEP” in Natal, Brazil. In particular, after some general thoughts on phenomenology we give a pedagogical introduction to the BFKL formalism and we discuss recent BFKL phenomenological studies for LHC observables.

PACS numbers: put PACS numbers here

1. Introduction

Phenomenology in its broader meaning, one would argue, has generally been instrumental in advancing the progress of human thought. Despite the fact that the etymology of the term, from the Greek words *phainómenon* and *lógos*, implies that phenomenology is the study of ‘that which is observed’, one has to stress that there is not a unique definition for phenomenology, or more accurately, that the definition varies a lot depending on the context (philosophy, psychology, science) and different people from different origins may associate different notions with the term.

If we restrict ourselves in seeking a definition for phenomenology within the grounds of modern physics, the following directive provides a possible candidate: “Observe ‘that which appears’, a collection of phenomena that share a unifying principle, and try to find patterns to describe it. The patterns might or might not be of fundamental nature or they might be up to a certain extend”. More specifically, for high energy physics, a possibly satisfactory statement could be the following: “Use assumed fundamental laws to produce theoretical estimates for physical observables and then compare against experimental data to validate or falsify the assumed laws”.

* Presented at the Summer School and Workshop on High Energy Physics at the LHC: New trends in HEP, October 21- November 6 2014, Natal, Brazil

In the past decades, high energy physics was mostly studied in colliders and the vast majority of experimentally measured quantities were observables stemming from the collision of particles. If the Standard Model (SM) enjoys such a wide acceptance as the correct theory for the description of the Strong and the Electroweak (EW) interactions, it has to do with a titanic effort from the experimental side (HERA, LEP, Tevatron, LHC) and an equally important effort from the theory community to provide theoretical estimates for a large amount of processes. The comparison between theory and experiment results in favor of the SM and so far no clear signal for new physics has emerged in any of the collision experiments. It will be very interesting to see whether the second run of the LHC could change this picture.

Apart from the (generally rare) times that an experimental situation is a standalone manifestation of a new phenomenon, it is usually after copious and demanding studies from both theoretical and experimental sides that one can speak about agreement or disagreement of the predictions with the data. Focusing hereafter on the theory side, we could argue that SM phenomenology actually means computing estimates for observables by employing perturbation theory since the SM Lagrangian cannot be solved exactly. We know that perturbation theory is only an approximation and cannot be applied without the presence of a small expansion parameter. The usual small parameter is the EW coupling in calculations in the EW sector of the SM and the strong coupling α_s in QCD. Moreover, in hadronic colliders, practically no physical observable lives solely in a region of the phase space¹ where non-perturbative input is unnecessary. This becomes evident for LHC observables if we think that the colliding particles are protons, objects of a non-perturbative nature due to their size and structure. Various factorization theorems and schemes are employed to put some order to that picture. The main idea behind factorization is that one separate the hard (perturbative) from the soft (non-perturbative) physics such that in order to have a theoretical estimate for an observable one needs to calculate the contribution from hard physics to that process and convolute it with a parametrization of the soft physics involved that takes into account all available data. The parametrization is based on the fact that soft physics can be in general process independent, e.g. the proton PDF's describe the probability to find a certain parton in the proton disregarding of the process in which the proton is involved.

The main bulk of phenomenological studies in the past decades is based on the so-called ‘fixed order’ calculations in which one considers only the

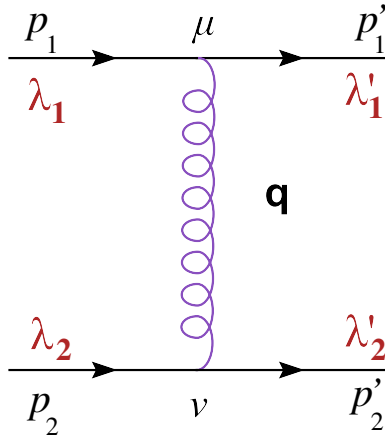
¹ The term “phase space” here is to be understood as a very wide notion: all possible configurations of initial conditions connected to all possible configurations of final states consist the phase space of observables.

first few terms of the perturbative expansion for a (hard) process and computes these terms fully. The perturbative expansion is realized via Feynman calculus and each term is graphically represented by Feynman diagrams. Assuming only the first term results to leading order (LO) calculations, assuming the first and second term results to next-to-leading (NLO) calculations, assuming the first three terms leads to next-to-next-to leading (NNLO) calculations and so forth. Most of the LHC processes require theoretical prediction at least to NLO and some of them to NNLO accuracy for a definite answer after comparing against experimental data. The complexity increases enormously as one goes from one order to the next and also as the number of external particles that participate in the process increases. Fixed order calculations justify fully their reputation of being ‘precision physics’ calculations since the only uncertainty that remains at the end is the uncertainty from omitting the higher term contributions and this can be well estimated in most cases².

In many cases, especially in hadron collider processes, not only a fixed order calculation is too complicated to be done beyond LO (e.g. multi-jet production) but also we have the presence of a large scale (usually the logarithm of a kinematical invariant or a mass) that persistently appears in every order combined with the small expansion parameter in a certain way and potentially could break down the convergence of the perturbative expansion. In such cases, we need a resummation scheme to sum all the large contributions from all terms (to order infinity). The result of the resummation can either be combined with a fixed order calculation or, if it encodes truly the most important contributions of each term in the expansion, it can be used alone as the theoretical estimate for a hard process. We should stress that any resummation approach is to be understood in the context of perturbation theory and also that each term of the perturbative expansion is represented by (effective) Feynman diagrams.

One of the most important resummation programs appears in the context of high energy scattering. If in a process the center-of-mass energy, \sqrt{s} , is really large then the product $(\alpha_s \ln s)$ can easily be of order unity. If in addition s is much larger than any other scale present, then in principle any term $\sim (\alpha_s \ln s)^n$, where n is arbitrarily high, would give the main contribution of the n -th term of the expansion and this term cannot be omitted. Instead, one has to resum all these important contributions up to $n \rightarrow \infty$. This is done within the Balitsky-Fadin-Kuraev-Lipatov (BFKL) formalism at leading logarithmic (LA) [1–4] and at next-to-leading logarithmic (NLA) accuracy [5,6]. For the latter, also terms that behave like $\alpha_s(\alpha_s \ln s)^n$ are re-

² There is also uncertainty from the non-perturbative input (e.g. PDF’s) but this is not directly connected to the fixed order calculation of the hard part of a process, or at least this is what factorization dictates.

Figure 1. qq -scattering at LO order.

summed. One sees thus, that resummation programs can also be regarded as a new perturbative expansion: the first term contains all the leading logarithmic terms to all orders (LO approximation), the second term the sub-leading logarithms (NLO corrections) and so on.

In the next section we will sketch a derivation of the BFKL equation that resums all large logarithms in s after introducing some important notions that are ubiquitous in the BFKL framework and of which the origin or the relevance are not obvious to the non-expert. In Section 3 we will discuss recent phenomenological studies for BFKL related observables and in Section 4 we will conclude with a general discussion.

2. The BFKL equation and the Pomeron

In this section, using a diagrammatic approach, our aim is to see

- How logarithms in s make their appearance in high energy scattering
- That these logarithms appear in all orders of the perturbative expansion
- How to resum these logarithms.

Setting our goals as listed above accounts as a minimal but hopefully an honest try to gain a first insight in BFKL physics. Following this course of reasoning though, will actually permit us to see a lot more, albeit on a very pedagogical level only. The ambitious reader who wants a deeper insight should consult more complete presentations of the topic, for example the

works in Refs. [7–12] and the original publications which arguably hide a richness of thought that cannot be covered in any review article.

Nevertheless, even in this minimalistic setting of goals as presented above and while we are chasing $(\alpha_s \ln s)^n$ -like terms in Feynman diagrams we will still be able to see

- How we separate virtual from real corrections and treat them in a separate manner and why this is of great importance.
- What the reggeization of the gluon is and pinpoint its origin.
- The different role of longitudinal and transverse degrees of freedom
- The “derivation” of the BFKL equation and its solution for the forward case.
- What the Pomeron is and whether we can describe it in a simple manner.

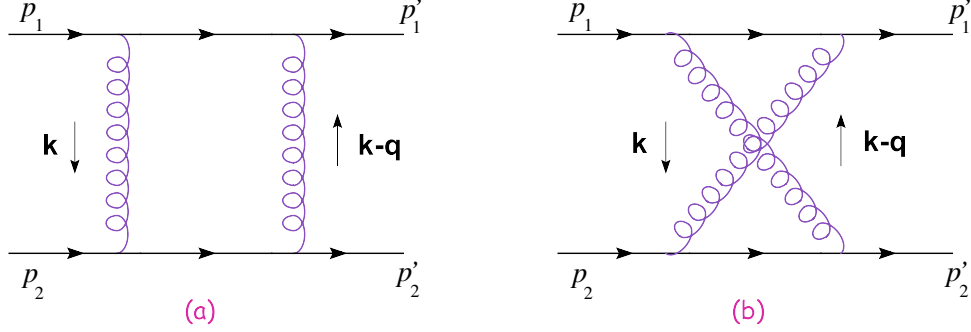
Let us start by considering qq -scattering at lowest order (Born level) as depicted in Fig. 1. Our discussion will be based a lot on the way the topic is presented in [7, 8]. Since we are concerned with high energy scattering, we will work in the high energy limit which is defined by the condition

$$s \gg |t|, \quad u \simeq -s. \quad (1)$$

The two quarks are interacting via a gluon exchange in the t -channel. We can write the momentum of the gluon in Sudakov parameters:

$$q = \rho p_1 + \sigma p_2 + q_\perp, \quad (2)$$

where p_1 and p_2 are the momenta of the incoming quarks and $q_\perp = (0, \mathbf{q}_\perp, 0)$ is a four-vector with non-zero entries for only the transverse part of the gluon momentum. To denote two-dimensional transverse vectors we use boldface characters hereafter. To keep contact with the physical picture of a collision in an experiment, any transverse momentum in the following should be understood as the projection of the total momentum on the transverse to the beam axis plane. Our kinematical invariants then expressed in Sudakov variables read: $s = 2p_1 p_2$ and $t = q^2 = \rho \sigma s - \mathbf{q}^2$. We should keep in mind that for perturbation theory to apply, we need the presence of a hard scale Q that will ensure the smallness of the strong coupling $\alpha_s(Q)$. We assume that such a scale exists but we leave it unidentified for the moment. Moreover, all factors in the formulae to follow that are irrelevant to the kinematics (such as color factors) will be suppressed.

Figure 2. qq -scattering, one-loop corrections.

For the upper vertex in Fig. 1 we have:

$$-ig_s \bar{u}(p_1 + q) \gamma_\mu u(p_1). \quad (3)$$

Because of Eq. 1, $q \ll p_1$ and the above formula can be approximated by

$$-ig_s \bar{u}(p_1) \gamma_\mu u(p_1) \simeq -2ig_s p_1^\mu. \quad (4)$$

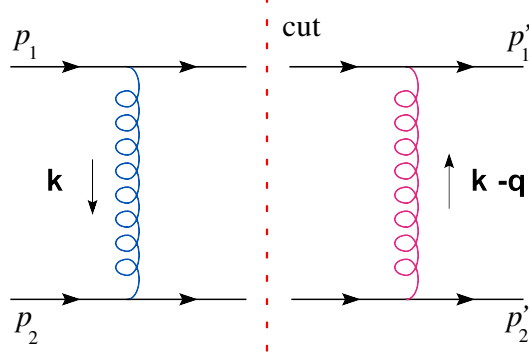
Approximating similarly the lower vertex, the amplitude for the process at hand at LO reads

$$A^{(0)}(s, t) = 8\pi a_s \mathcal{CF}_1 \frac{s}{q^2} = 8\pi a_s \mathcal{CF}_1 \frac{s}{t}. \quad (5)$$

where \mathcal{CF}_1 denotes a color factor. We see that there are no logarithms in s in Eq. 5 as was easy to guess beforehand. We would like now to move to the next order and consider diagrams that stem from the tree diagram after attaching another gluon. This new gluon can either be virtual, in which case we will have one-loop diagrams (virtual radiative corrections), or it can be real which would mean that it could in principle be detected in the final state (real corrections). Instead of considering both real and virtual corrections simultaneously at NLO, we will follow a different course. We will consider first only the virtual correction, first at NLO, then at NNLO and see where this approach can take us.

It turns out that one-loop diagrams with self-energy and vertex corrections are sub-leading in $\ln s$ and do not need to be computed. Only box diagrams are contributing and the ones that give the relevant $\ln s$ term are shown in Fig. 2. Let us focus on the Fig. 2(a) diagram. We can calculate its imaginary part using the Cutkosky rules (see Fig 3) and then obtain the full amplitude by dispersion relations. Denoting the NLO amplitude by $A^{(1)}(s, t)$ we have:

$$\text{Im} A^{(1)}(s, t) = \frac{1}{2} \int d\text{PS}^{(2)} A^{(0)}(s, k^2) A^{(0)\dagger}(s, (k - q)^2), \quad (6)$$


 Figure 3. qq -scattering, one-loop cut amplitude.

where $A^{(0)}(s, k^2)$ and $A^{(0)\dagger}(s, (k-q)^2)$ are the tree level amplitudes in Fig. 3 with the quark lines being on shell at the cut points. $A^{(0)\dagger}$ stands for the hermitian conjugate of $A^{(0)}$. The two-body phase space $\int d\text{PS}^{(2)}$ is given by

$$\int d\text{PS}^{(2)} = \int \frac{d^4 k}{(2\pi)^2} \delta((p_1 - k)^2) \delta((p_2 + k)^2). \quad (7)$$

Again, by introducing Sudakov variables ρ, σ we can express k and $d^4 k$ as

$$k = \rho p_1 + \sigma p_2 + k_\perp, \quad d^4 k = \frac{s}{2} d\rho d\sigma d^2 \mathbf{k}. \quad (8)$$

so that we finally obtain for the two-body phase space:

$$\int d\text{PS}^{(2)} = \frac{1}{8\pi^2 s} \int d^2 \mathbf{k}. \quad (9)$$

The two tree level amplitudes in Eq. 6 read

$$A^{(0)}(s, k^2) = -8\pi a_s \mathcal{CF}_2 \frac{s}{\mathbf{k}^2} \quad (10)$$

and

$$A^{(0)\dagger}(s, (k-q)^2) = -8\pi a_s \mathcal{CF}_3 \frac{s}{(\mathbf{k}-\mathbf{q})^2}, \quad (11)$$

where \mathcal{CF}_2 and \mathcal{CF}_3 are color factors. The imaginary part of $A^{(0)}(s, t)$, with the help of Eq. 9, becomes:

$$\text{Im} A^{(1)}(s, t) = 4\alpha_s^2 s \mathcal{CF}_4 \int \frac{d^2 \mathbf{k}}{\mathbf{k}^2 (\mathbf{k}-\mathbf{q})^2} \quad (12)$$

and by dispersion relations we can reconstruct the full amplitude which reads:

$$A^{(1)}(s, t) = -4 \frac{\alpha_s^2}{\pi} \mathcal{CF}_4 \ln\left(\frac{s}{t}\right) s \int \frac{d^2 \mathbf{k}}{\mathbf{k}^2 (\mathbf{k} - \mathbf{q})^2}. \quad (13)$$

We remind the reader that we are tracing leading logarithms in s , and since $s/t < 0$ we can write for a generic amplitude $\mathcal{A} \sim \mathcal{B} \ln \frac{s}{t}$ after making the decomposition into real and imaginary parts:

$$\mathcal{A} = \text{Re}\mathcal{A} + i \text{Im}\mathcal{A} \sim \mathcal{B} \ln \frac{s}{t} = \mathcal{B} \ln \frac{s}{|t|} - i\pi \mathcal{B} \quad (14)$$

which simply means $\text{Re}\mathcal{A} = -\frac{1}{\pi} \text{Im}\mathcal{A} \ln \frac{s}{|t|}$. Thus, after defining

$$\epsilon(t) = \frac{N_c \alpha_s}{4\pi^2} \int -\mathbf{q}^2 \frac{d^2 \mathbf{k}}{\mathbf{k}^2 (\mathbf{k} - \mathbf{q})^2}, \quad (15)$$

where the function $\epsilon(t)$ is called gluon Regge trajectory, we rewrite Eq. 13 as

$$A^{(1)}(s, t) = -\frac{16\pi\alpha_s}{N_c} \mathcal{CF}_4 \frac{s}{t} \ln\left(\frac{s}{t}\right) \epsilon(t), \quad (16)$$

whereas for the Fig. 2(b) diagram in the crossed channel it will be:

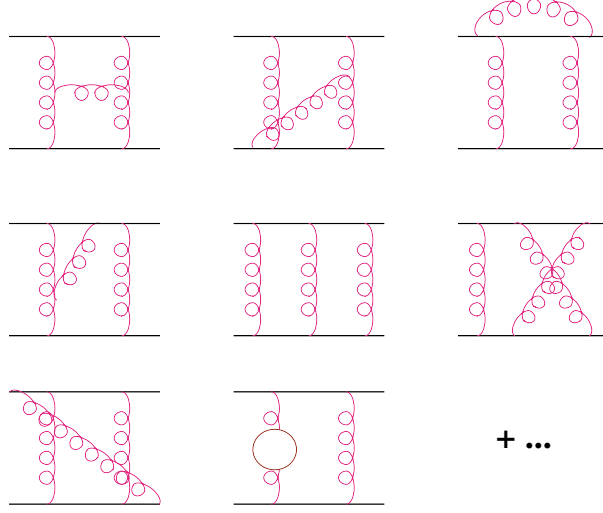
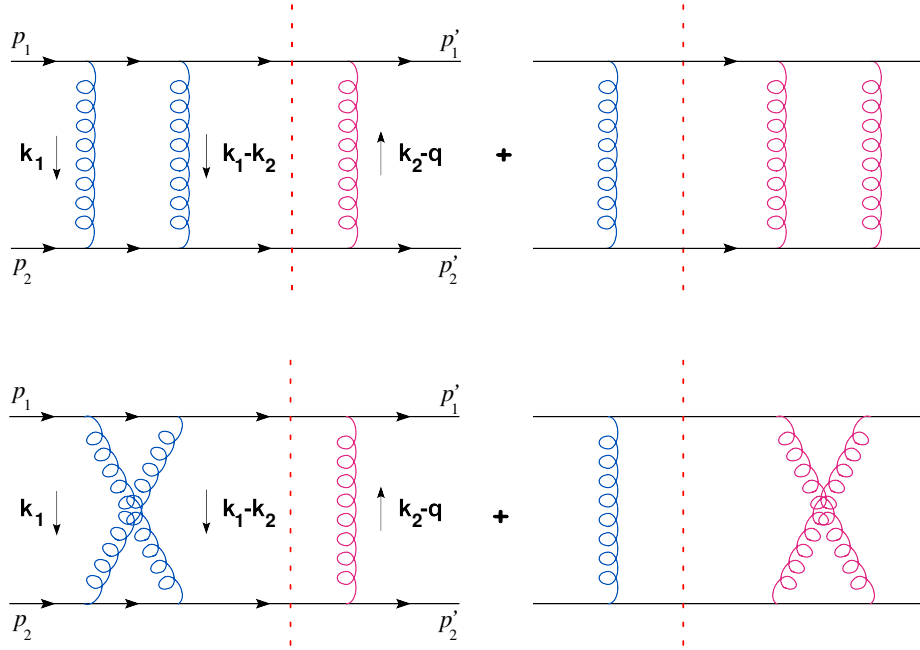
$$A_{\text{cross}}^{(1)}(s, t) = -\frac{16\pi\alpha_s}{N_c} \mathcal{CF}_5 \frac{u}{t} \ln\left(\frac{u}{t}\right) \epsilon(t). \quad (17)$$

After adding the last two equations and using $u \simeq -s$, we obtain the one-loop amplitude. Considering colour octet exchange³, we can express the one-loop amplitude in terms of the tree level one, specifically:

$$A_s^{(1)}(s, t) = 8\pi a_s \mathcal{CF}_1 \frac{s}{t} \ln\left(\frac{s}{|t|}\right) \epsilon(t) = A^{(0)} \ln\left(\frac{s}{|t|}\right) \epsilon(t). \quad (18)$$

One order higher in the perturbative expansion, to $\mathcal{O}(\alpha_s^3)$, we have to consider many Feynman diagrams like the ones in Fig. 4. Not all of them though contribute with leading logarithms. The ones we need to compute are box diagrams, in particular, the two-loop box diagrams in Fig. 5. Using the Cutkosky rules again, we can express the two-loop diagrams into one-loop and tree contributions that are known from the analysis so far. Indeed, in Fig 5, after multiplying the amplitudes to the left of the cut line by the (hermitian conjugates of) the ones to the right, summing over helicities

³ We have hidden any color dependence of the amplitudes in the color factors \mathcal{CF}_i , any reader interested in color decomposition should consult Ref. [9], in particular, Section 9.4.3.


 Figure 4. qq -scattering, two-loop diagrams.

 Figure 5. qq -scattering, two-loop box virtual corrections.

and performing the integration over the phase space, we reach the very

interesting result:

$$A_8^{(2)}(s, t) = A^{(0)}(s, t) \frac{1}{2} \ln^2\left(\frac{s}{|t|}\right) \epsilon^2(t), \quad (19)$$

where the two-loop amplitude is expressed in terms of the LO one. The expressions for $A_8^{(2)}(s, t)$ and $A_8^{(1)}(s, t)$ tell us that the partial result for the amplitude up to order $\mathcal{O}(\alpha_s^3)$ is

$$A_8^{\text{partial}}(s, t) = A^{(0)}(s, t) \left(1 + \ln\left(\frac{s}{|t|}\right) \epsilon(t) + \frac{1}{2} \ln^2\left(\frac{s}{|t|}\right) \epsilon^2(t) \right). \quad (20)$$

suggesting that the all-orders virtual amplitude might be of the form

$$A_8(s, t) = A^{(0)}(s, t) \left(1 + \ln\left(\frac{s}{|t|}\right) \epsilon(t) + \frac{1}{2} \ln^2\left(\frac{s}{|t|}\right) \epsilon^2(t) + \dots \right), \quad (21)$$

namely, a product of the tree level amplitude and something that looks very much like a series expansion. From that point on, it only takes a small logical step to postulate that

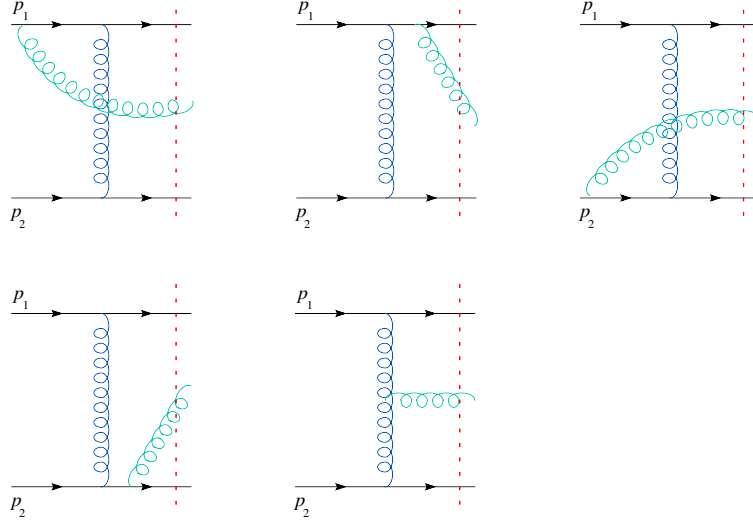
$$A_8(s, t) = A^{(0)}(s, t) \left(\frac{s}{|t|} \right)^{\epsilon(t)}. \quad (22)$$

It is impressive to know that the ansatz in Eq. 22 is proven to be true by the so-called bootstrap equation.

At this point, we have partially achieved one of our primary goals, we have seen how logarithms in s appear in virtual diagrams in different orders of the perturbative expansion and we have managed to resum them in a closed form to all orders. The final result can be written in a factorized form involving two terms, the Born amplitude and the expression $\left(\frac{s}{|t|}\right)^{\epsilon(t)}$ which accounts for the resummation of the large energy logarithms. We can actually obtain Eq. 22 by going back to Fig. 1 and calculating the tree level amplitude using for the t -channel gluon a modified propagator which would read:

$$D_{\mu\nu}(s, q^2) = -i \frac{g_{\mu\nu}}{q^2} \left(\frac{s}{\mathbf{k}^2} \right)^{\epsilon(q^2)}. \quad (23)$$

Eq. 23 states that in the high energy limit, in order to take into account all the important contributions from virtual diagrams to all orders it suffices to calculate the tree level amplitude using a modified propagator for the t -channel gluon. The importance of this striking result cannot be overestimated. The gluon with the modified propagator is called a reggeized gluon


 Figure 6. qq -scattering, one real gluon emission.

or Reggeon and it hints that the relevant degrees of freedom in high energy scattering might not be just quarks and gluons.

Let us now focus on the real corrections and in particular the real gluon emission diagrams in Fig. 6 which are the first real emission corrections to the Born amplitude. Formally these are $\mathcal{O}(\alpha_s^3)$ corrections.

It turns out that instead of calculating the amplitudes for all those diagrams it suffices to substitute their contribution by the diagram in Fig. 7 where the blob stands for the Lipatov effective vertex which is gauge invariant and has a tensorial structure. The Lipatov effective vertex sums the contributions from the graphs in Fig. 6 in an elegant way. Using once more Sudakov decomposition, the momenta of the two t -channel gluons in Fig. 7 read

$$\begin{aligned} k_1 &= \rho_1 p_1 + \sigma_1 p_2 + k_{1\perp} \\ k_2 &= \rho_2 p_1 + \sigma_2 p_2 + k_{2\perp}, \end{aligned} \quad (24)$$

and the relevant kinematical limit is given by the following conditions:

$$\begin{aligned} 1 &\gg \rho_1 \gg \rho_2 \\ 1 &\gg |\sigma_2| \gg |\sigma_1| \end{aligned} \quad (25)$$

Using the Cutkosky rules once more, we contract the tree level amplitude from the diagram in Fig. 7 with its hermitian conjugate and we integrate

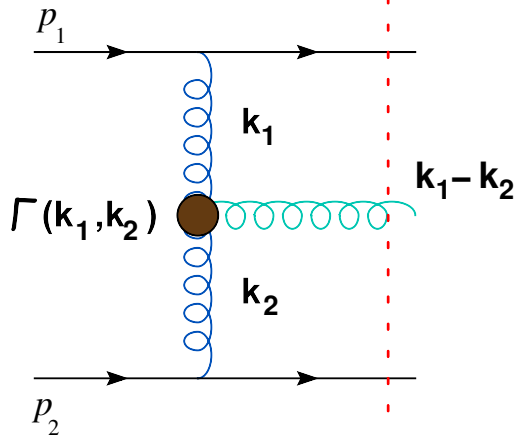


Figure 7. The Lipatov effective vertex.

over the three-body phase space which in our Sudakov parametrization reads

$$\int d\text{PS}^{(3)} = \frac{s^2}{4(2\pi)^5} \int d\rho_1 d\rho_2 d\sigma_1 d\sigma_2 d^2\mathbf{k}_1 d^2\mathbf{k}_2 \delta(-\sigma_1(1-\rho_1)s - \mathbf{k}_1^2) \delta(\rho_2(1+\sigma_2)s - \mathbf{k}_2^2) \delta((\rho_1 - \rho_2)(\sigma_1 - \sigma_2)s - (\mathbf{k}_1 - \mathbf{k}_2)^2). \quad (26)$$

Because of Eq. 25 we may use the following approximations:

$$\begin{aligned} 1 - \rho_1 &\simeq 1, \\ 1 + \sigma_2 &\simeq 1, \\ \rho_1 - \rho_2 &\simeq \rho_1, \quad \sigma_1 - \sigma_2 \simeq -\sigma_2, \end{aligned} \quad (27)$$

so that Eq. 26 now reads

$$\int d\text{PS}^{(3)} = \frac{s^2}{4(2\pi)^5} \int d\rho_1 d\rho_2 d\sigma_1 d\sigma_2 d^2\mathbf{k}_1 d^2\mathbf{k}_2 \delta(-\sigma_1 s - \mathbf{k}_1^2) \delta(\rho_2 s - \mathbf{k}_2^2) \delta(-\rho_1 \sigma_2 s - (\mathbf{k}_1 - \mathbf{k}_2)^2). \quad (28)$$

It is from the rightmost delta function in (Eq. 28) that the $\ln s$ behavior of the real corrections arises. Indeed, after carrying out the integration over σ_2 , the remaining integrand will acquire an $(1/\rho_1)$ factor:

$$\int d\text{PS}^{(3)} = \frac{1}{4(2\pi)^5 s} \int_{\mathbf{k}_2^2/s}^1 \frac{d\rho_1}{\rho_1} \int d^2\mathbf{k}_1 d^2\mathbf{k}_2 \quad (29)$$

and finally performing the ρ_1 integration yields a factor

$$\ln \left(\frac{s}{\mathbf{k}_2^2} \right) = \ln \left(\frac{s}{s_0} \right), \quad (30)$$

where s_0 is a typical momentum, a typical normalisation scale.

To consider one order higher corrections, we need to consider two real gluon emissions. The diagrammatic depiction would be the one in Fig 7 but now with two Lipatov effective vertices and three gluon propagators in the t -channel. We would need to integrate over the four-body phase space in order to get the leading logarithms in s . It is straightforward to generalise this procedure for three, four and finally an arbitrary number of real gluon emissions. We would like at this point to find a way to combine the real with the virtual corrections and most importantly, to find a way to account for the real emission corrections to all orders in an closed form expression.

Let us recapitulate here what insight we have gained and assess where we stand with regard to our initial aims. In the discussion about the virtual corrections, we have introduced the notion of gluon reggeization: a t -channel gluon with a modified propagator defined as in Eq. 23 takes into account the leading logarithmic contributions from virtual diagrams to all orders. This is the closest one can have for a recipe: to account for virtual corrections, substitute the t -channel gluon by a Reggeon. On the other hand, the idea of combining the various one real emission diagrams into a single diagram where we consider one gluon emission in the s -channel that connects to the t -channel gluon by means of a Lipatov effective vertex allows for the iteration of this prescription to cover an arbitrary high n -gluon emissions. All these lead very naturally to what we call ladder diagrams, an example is depicted in Fig. 8. This is the general picture of a BFKL ladder in the colour singlet exchange, and a graphical depiction of what we call the perturbative Pomeron. Let us have a closer view at the diagram in Fig 8. It consists of n rungs (real emitted gluons) connected to the t -channel reggeized gluons (zig-zag lines) via Lipatov effective vertices. The t -channel gluons are partitioned into $n + 1$ reggeized propagators. The imaginary part of the amplitude, $\text{Im}\mathcal{A}(s, t)$ for a process like that will be given by convoluting the two tree level amplitudes (left and right to the cut) and after integrating over the $n + 2$ -body phase space. The generalisation of the condition in Eq. 1, leads to the kinematical configuration called multi-Regge kinematics (MRK):

$$\begin{aligned} \mathbf{k}_1^2 &\simeq \mathbf{k}_2^2 \simeq \dots \simeq \mathbf{k}_i^2 \simeq \mathbf{k}_{i+1}^2 \dots \simeq \mathbf{k}_n^2 \simeq \mathbf{k}_{n+1}^2 \gg \mathbf{q}^2 \simeq s_0, \\ 1 &\gg \rho_1 \gg \rho_2 \gg \dots \rho_i \gg \rho_{i+1} \gg \rho_{n+1} \gg \frac{s_0}{s}, \\ 1 &\gg |\sigma_{n+1}| \gg |\sigma_n| \gg \dots \gg |\sigma_2| \gg |\sigma_1| \gg \frac{s_0}{s}. \end{aligned} \quad (31)$$

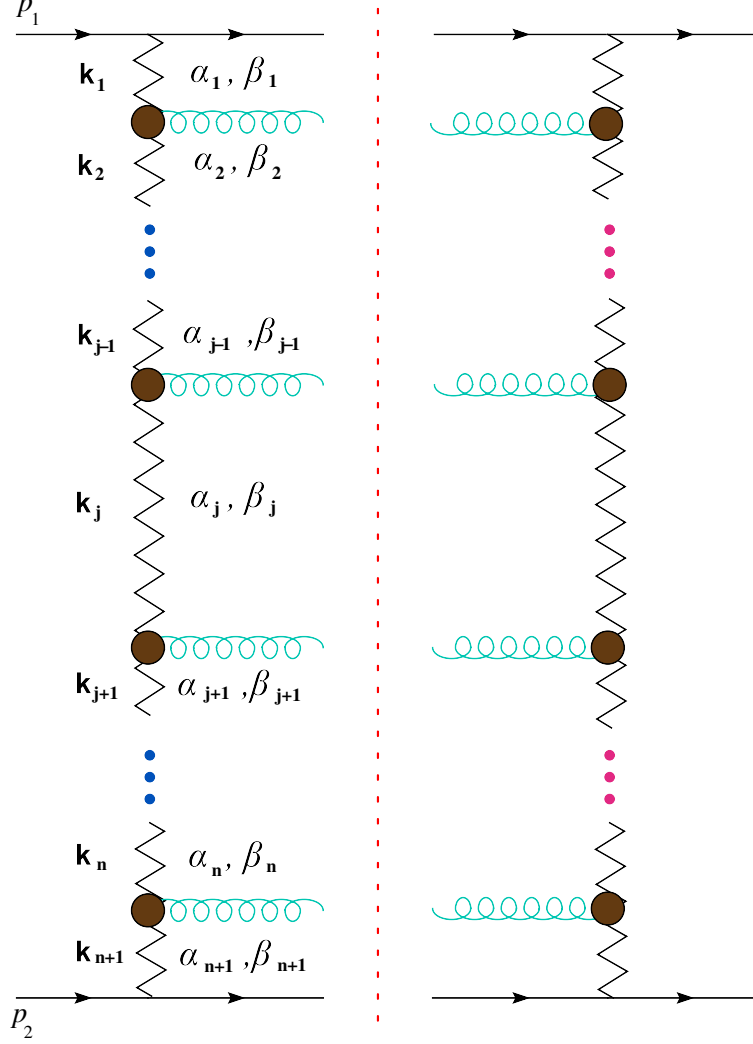


Figure 8. A typical gluonic ladder diagram.

The nested integration over the phase space is a nuisance and the way out is to turn the multi-nested integral into a product of integrals by taking the Mellin transform of $\text{Im}\mathcal{A}(s, t)$ working thus, in the complex angular momentum space ω :

$$f(\omega, t) = \int_1^\infty d\left(\frac{s}{s_0}\right) \left(\frac{s}{s_0}\right)^{-\omega-1} \frac{\text{Im}\mathcal{A}(s, t)}{s}. \quad (32)$$

$f(\omega, t)$ can be the starting point from which we further define a function $f_\omega(\mathbf{k}_a, \mathbf{k}_b, t)$ which, as its arguments suggest, is the Mellin transform of the amplitude with the integrations over the transverse momenta \mathbf{k}_a and \mathbf{k}_b still to be performed, where \mathbf{k}_a and \mathbf{k}_b are the topmost and bottommost reggeized gluon propagators in the ladder. The function $f_\omega(\mathbf{k}_a, \mathbf{k}_b, t)$ is the so-called BFKL Green's function. Since $t \simeq -\mathbf{q}^2$, we will prefer the notation $f_\omega(\mathbf{k}_a, \mathbf{k}_b, \mathbf{q}^2)$ in the following, in which the propagators \mathbf{k}_a and $(\mathbf{q} - \mathbf{k}_b)^2$ are contained and with \mathbf{q}^2 we denote the momentum transfer in the t -channel. One could then take $n = 1$ in the ladder diagram in Fig. 8 and calculate the corresponding $f_\omega^{(1)}(\mathbf{k}_a, \mathbf{k}_b, \mathbf{q}^2)$ function and then set $n = 2$ and calculate the $f_\omega^{(2)}(\mathbf{k}_a, \mathbf{k}_b, \mathbf{q}^2)$ and after iterating this procedure up to an arbitrary $n \rightarrow \infty$ and summing up all contributions, one would compute $f_\omega(\mathbf{k}_a, \mathbf{k}_b, \mathbf{q}^2)$. Easy to describe but impossible to do. Instead, there is an elegant way through. After taking the Mellin transform in Eq. 32 and writing the generic expression for $f_\omega(\mathbf{k}_a, \mathbf{k}_b, \mathbf{q}^2)$ with the phase space integration still to be done, one realizes⁴ that there exists an integral equation which governs the behavior of f_ω :

$$\begin{aligned} \omega f_\omega(\mathbf{k}_a, \mathbf{k}_b, \mathbf{q}) &= \delta^2(\mathbf{k}_a - \mathbf{k}_b) \\ &+ \frac{\bar{\alpha}_s}{2\pi} \int d^2\mathbf{l} \left\{ \frac{-\mathbf{q}^2}{(1 - \mathbf{q})^2 \mathbf{k}_a^2} f_\omega(\mathbf{l}, \mathbf{k}_b, \mathbf{q}) \right. \\ &+ \frac{1}{(1 - \mathbf{k}_a)^2} \left(f_\omega(\mathbf{l}, \mathbf{k}_b, \mathbf{q}^2) - \frac{\mathbf{k}_a^2 f_\omega(\mathbf{k}_a, \mathbf{k}_b, \mathbf{q})}{\mathbf{l}^2 + (\mathbf{k}_a - \mathbf{l})^2} \right) \\ &+ \frac{1}{(1 - \mathbf{k}_a)^2} \left(\frac{(\mathbf{k}_a - \mathbf{q})^2 \mathbf{l}^2 f_\omega(\mathbf{l}, \mathbf{k}_b, \mathbf{q}^2)}{(1 - \mathbf{q})^2 \mathbf{k}_a^2} \right. \\ &\quad \left. \left. - \frac{(\mathbf{k}_a - \mathbf{q})^2 f_\omega(\mathbf{k}_a, \mathbf{k}_b, \mathbf{q}^2)}{(1 - \mathbf{q})^2 (\mathbf{k}_a - \mathbf{l})^2} \right) \right\}, \end{aligned} \quad (33)$$

with $\bar{\alpha}_s = N_c \alpha_s / \pi$. This is the BFKL equation. In the case of zero momentum transfer, $\mathbf{q}^2 = 0$, Eq. 33 becomes:

$$\begin{aligned} \omega f_\omega(\mathbf{k}_a, \mathbf{k}_b) &= \delta^2(\mathbf{k}_a - \mathbf{k}_b) \\ &+ \frac{\bar{\alpha}_s}{2\pi} \int \frac{d^2\mathbf{l}}{(1 - \mathbf{k}_a)^2} \left(f_\omega(\mathbf{l}, \mathbf{k}_b) - \frac{\mathbf{k}_a^2 f_\omega(\mathbf{k}_a, \mathbf{k}_b)}{\mathbf{l}^2 + (\mathbf{k}_a - \mathbf{l})^2} \right). \end{aligned} \quad (34)$$

The impossible task of summing an infinite number of integrals, each one with a $(i + 1)$ -body phase space if its previous has an i -body phase

⁴ To demonstrate that, one needs to go through the calculation which is beyond our scope here. The reader is encouraged to try it out with the help of the references cited in the beginning of the section in order to see how magic works.

space turns into finding a way to solve Eq. 33. We can rewrite the BFKL equation in a more symbolic form as

$$\omega f_\omega(\mathbf{k}_a, \mathbf{k}_b) = \delta^2(\mathbf{k}_a - \mathbf{k}_b) + \int d^2\mathbf{l} \mathcal{K}(\mathbf{k}_a, \mathbf{l}) f_\omega(\mathbf{l}, \mathbf{k}_b), \quad (35)$$

where $\mathcal{K}(\mathbf{k}_a, \mathbf{l})$ is the BFKL kernel:

$$\mathcal{K}(\mathbf{k}_a, \mathbf{l}) = \underbrace{2\epsilon(-\mathbf{k}^2) \delta^2(\mathbf{k}_a - \mathbf{l})}_{\mathcal{K}_{virt}} + \underbrace{\frac{N_c \alpha_s}{\pi^2} \frac{1}{(\mathbf{k}_a - \mathbf{k}_b)^2}}_{\mathcal{K}_{real}}. \quad (36)$$

\mathcal{K}_{virt} and \mathcal{K}_{real} are the parts of the kernel that correspond to the virtual and real corrections respectively.

Solving the BFKL equation will provide us with the BFKL gluon Green's function from which we can reconstruct the imaginary part of the amplitude for qq -scattering in two steps. First, we need to perform the inverse Mellin transform to return to s space:

$$f(s, \mathbf{k}_a, \mathbf{k}_b, \mathbf{q}) = \frac{1}{2\pi i} \int_{c-i\infty}^{c+i\infty} d\omega \left(\frac{s}{s_0} \right)^\omega f_\omega(\mathbf{k}_a, \mathbf{k}_b, \mathbf{q}) \quad (37)$$

and subsequently we need to integrate over the \mathbf{k}_a and \mathbf{k}_b momenta of the reggeized gluons:

$$\mathcal{A}_{\text{singlet}}(s, t) = i(8\pi\alpha_s)^2 s \frac{N_c^2 - 1}{4N_c^2} \int \frac{d^2\mathbf{k}_a}{(2\pi)^2} \frac{d^2\mathbf{k}_b}{(2\pi)^2} \frac{f(s, \mathbf{k}_a, \mathbf{k}_b, \mathbf{q})}{\mathbf{k}_b^2 (\mathbf{k}_a - \mathbf{q})^2}, \quad (38)$$

where we kept the color factor for qq -scattering explicit.

The amplitude in Eq. 38 is the amplitude for scattering via a perturbative Pomeron exchange. If nature were to follow the BFKL dynamics, or more precisely, in the kinematical limit where BFKL dynamics is dominant and describes fully the perturbative QCD picture, the interaction between two quarks would be the outcome of summing all possible ladder diagrams with n -rungs, $n \rightarrow \infty$, and this would be the equivalent of saying that the two quarks exchange a Pomeron. This is obviously not a definition of the Pomeron but describes a good deal of how to perceive it in an intuitive manner.

The BFKL kernel in Eq. 36 is infrared finite, \mathcal{K}_{real} and \mathcal{K}_{virt} are both singular but their divergencies cancel one against the other. The amplitude though is still infrared divergent due to the gluon propagators $\frac{1}{\mathbf{k}_b^2}$ and $\frac{1}{(\mathbf{k}_a - \mathbf{q})^2}$. In practice, the quarks (or scattering gluons for that matter) are

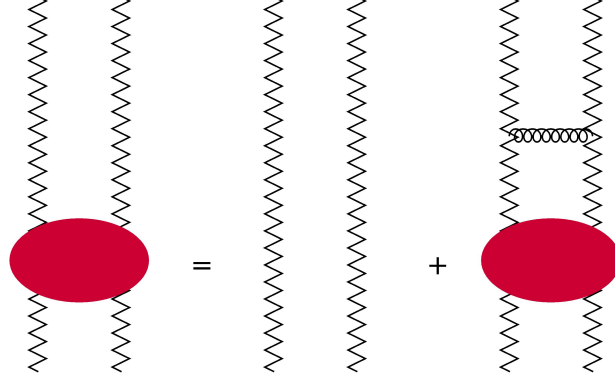


Figure 9. Graphical depiction of the BFKL equation.

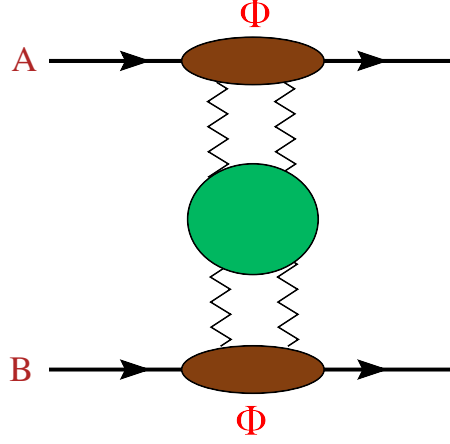


Figure 10. High energy hadron-hadron scattering. The interaction factorizes into the process independent part which is the BFKL gluon Green's function (green blob) and the its effective couplings to the scattering projectiles, the impact factors (brown blobs).

not on mass-shell as we presupposed in the discussion of the BFKL equation so far. In physical processes, as for example in hadron hadron collisions at the LHC, the Pomeron couples to off shell partons inside a hadron. To account for the hadronic structure, we need to introduce the notion of the impact factor, Φ , which is practically the coupling of the Pomeron to the hadron. Then a hadronic elastic amplitude between hadrons A and B (Fig. 10) will be written as

$$\mathcal{A}(s, t) = i s C \int \frac{d^2 \mathbf{k}_a}{(2\pi)^2} \frac{d^2 \mathbf{k}_b}{(2\pi)^2} \Phi_A(\mathbf{k}_a, \mathbf{q}) \frac{f(s, \mathbf{k}_a, \mathbf{k}_b, \mathbf{q})}{\mathbf{k}_b^2 (\mathbf{k}_a - \mathbf{q})^2} \Phi_B(\mathbf{k}_b, \mathbf{q}), \quad (39)$$

where \mathcal{C} accounts for the colour factor of the process⁵ and the quantities Φ_A and Φ_B are the hadron impact factors for the hadrons A and B . Whenever we have a Pomeron exchange in particle scattering, we need also to include in the analysis the impact factors for each of the scattering parts. In general, impact factors are process dependent object and mostly of non perturbative nature and thus non-calculable and subjects to modelling. Still, there has been quite significant effort by the community to calculate perturbative impact factors to NLO [13–34]. Nevertheless, all impact factors have to share a very important universal behavior, i.e. they become zero in the limits

$$\Phi(\mathbf{k}, \mathbf{q}) \Big|_{\mathbf{k} \rightarrow 0}^{\mathbf{k} - \mathbf{q} \rightarrow 0} \rightarrow 0. \quad (40)$$

and they regulate thus the infrared divergencies of Eq. 39 which exactly appear in these limits.

We can rewrite Eq. 35 as

$$\omega F = \mathcal{I} + \mathcal{K} \otimes F, \quad (41)$$

with \mathcal{K} being the BFKL kernel as in Eq. 36, and attempt to diagonalise the BFKL equation by finding the eigenfunctions ϕ_a of the kernel \mathcal{K}

$$\mathcal{K} \otimes \phi_a = \omega_a \phi_a. \quad (42)$$

If θ is the azimuthal angle of the momenta, then the eigenfunctions can be written as:

$$\phi_{n\nu}(|\mathbf{k}|, \theta) = \frac{1}{\pi\sqrt{2}} (\mathbf{k}^2)^{-\frac{1}{2}+i\nu} e^{in\theta}. \quad (43)$$

The high energy behavior of the total cross section is determined by the behavior of the angular averaged kernel (averaged over the azimuthal angle between \mathbf{k}_a and \mathbf{k}_b) and then $(\mathbf{k}^2)^{\gamma-1}$ can be used as eigenfunctions such that:

$$\int d^2k \mathcal{K}(\mathbf{k}_a, \mathbf{k}) (\mathbf{k}^2)^{\gamma-1} = \frac{N_c \alpha_s}{\pi} \chi_0(\gamma) (\mathbf{k}_a^2)^{\gamma-1} \quad (44)$$

with eigenvalues

$$\omega_n(\gamma) = \frac{\alpha_s N_c}{\pi} \left(2\psi(1) - \psi\left(\gamma + \frac{n}{2}\right) - \psi\left(1 - \gamma + \frac{n}{2}\right) \right), \quad \psi(\gamma) = \Gamma'(\gamma)/\Gamma(\gamma)$$

⁵ For example, $\mathcal{C} = (N_c^2 - 1)/4N_c^2$ for qq -scattering

and $\gamma = 1/2 + i\nu$. The set of eigenfunctions is complete with ν taking real values between $-\infty$ and ∞ . The solution can therefore be expressed using the expansion on the eigenfunctions and reads

$$f(\mathbf{k}_a, \mathbf{k}_b, Y) = \frac{1}{\pi \mathbf{k}_a \mathbf{k}_b} \sum_{n=-\infty}^{\infty} \int \frac{d\omega}{2\pi i} e^{\omega Y} \int \frac{d\gamma}{2\pi i} \left(\frac{\mathbf{k}_a^2}{\mathbf{k}_b^2} \right)^{\gamma - \frac{1}{2}} \frac{e^{in\theta}}{\omega - \omega_n(\alpha_s, \gamma)}, \quad (45)$$

where $Y = \ln \left(\frac{s}{s_0} \right)$ is the rapidity interval between \mathbf{k}_a and \mathbf{k}_b . Eq. 45 makes apparent the distinct power-like growth with energy prediction within the BFKL dynamics that characterises the behavior of the cross sections at large energies. The relevant term here is $e^{\omega Y}$.

So far, we have encountered a number of important features of the BFKL resummation program all seen at leading logarithmic accuracy. At next-to-leading logarithmic approximation (NLLA), it turns out that the reggeization of the gluon still holds which is a key point. It means that one can use the leading order form of BFKL equation changing only the kernels and the eigenvalues [5]. We will not discuss in any detail the NLO BFKL equation here. We will only sketch the origin of the terms $\alpha_s(\alpha_s \ln s)^n$ and we will mention a couple of important points for BFKL phenomenology.

The NLO⁶ corrections stem from two different kinematical configurations. In MRK, the next-to-leading order corrections for the gluon Regge trajectory as well as the virtual corrections to the Reggeon-Reggeon- g vertex have to be included. The reggeized gluon trajectory has to be calculated at two-loop approximation, $\epsilon^{(2)}$ [35], whereas, the real part of the kernel, $\mathcal{K}_{\text{real}}$ gets contributions from one-loop level gluon production [36].

One can also obtain a term of the type $\alpha_s(\alpha_s \ln s)^n$ starting from an amplitude at LLA and after losing a relative $\ln s$ term. We saw that the key feature that generates these logarithmic terms is the strong ordering of the emitted gluons in rapidity space. Thus, if we allow for a state in which two of the emitted particles are close in rapidity, we are in the Quasi-Multi-Regge-kinematics (QMRK) where Eq. 31 still holds with the exception of a pair of particles. The pair can be a pair of gluons or a $q\bar{q}$ pair [37, 38] (Fig. 11).

The calculation of the NLLA corrections was an difficult task that took almost a decade [5, 6]. After its completion, it turned out that the NLLA corrections compared to the LLA term were very large questioning the convergence itself of the perturbative expansion in terms of $(\alpha_s \ln s)$. The problem has its origin to the fact that since the transverse momenta of the emitted

⁶ As mentioned in the introduction, in the field, there is an interchangeability between the terms ‘NLL’ and ‘NLO’. We will follow the practise here with the assurance that by now the context makes clear what one really means.

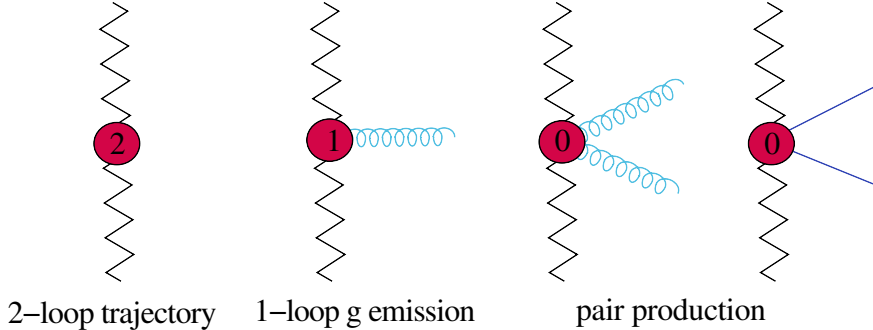


Figure 11. Schematic representation of the configurations that contribute to the NLLA approximation.

gluons are not restricted, there can be final states in which the transverse momenta are strongly ordered. This in turn means that large logarithms of transverse momenta (collinear logarithms) can be present and render the expansion in $(\alpha_s \ln s)$ terms unstable. Therefore, one needs to perform a complete collinear resummation of these large logarithms in order to stabilize the convergence of the expansion [39].

3. BFKL phenomenology at the LHC

In the past thirty years, a number of probes of BFKL physics have been proposed for different collider environments. Actually, BFKL phenomenology had its first major flourish in the nineties, especially after HERA at DESY started producing data for the proton structure function F_2 that were showing a power-like rise with decreasing x , the Bjorken scaling variable. Since the early HERA days, much of the progress seen on more formal theoretical issues regarding the BFKL formalism was driven from a need to compare against experimental measurements. Nevertheless, the absence of a clear signal that would only be described by BFKL physics and by nothing else was a drawback. Despite the big progress in the field, most of the studies we still have are beyond LO but only a few calculations provide full NLO accuracy estimates within the BFKL framework.

Nowadays, the general consensus is that one should apply the BFKL formalism to processes that have two hard scales at the two ends of the BFKL ladder that are of the same magnitude. Otherwise, if there is strong ordering in the transverse momentum of the two scales, DGLAP [40–42] logarithms appear and BFKL is not any more the only relevant framework. A very strict list of probes would include the processes $\gamma^* \gamma^* \rightarrow \text{hadrons}$ in a e^+e^- collider, forwards jets in Deep Inelastic Scattering (DIS) at HERA,

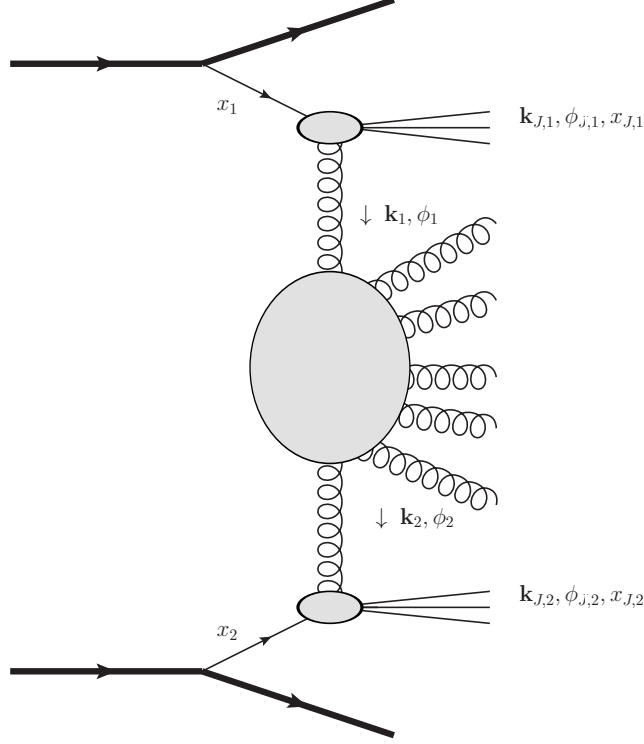


Figure 12. The kinematics of Mueller-Navelet jets. Figure taken from Ref. [51].

Mueller-Navelet jets and Mueller-Tang jets at hadron colliders (Tevatron, LHC). We do not include in the list the F_2 behavior in DIS which is also driven by non-perturbative physics. From the list of probes above, Mueller-Navelet jets [43] is the observable that has received most of the theoretical attention in recent years as the process can be studied experimentally at the LHC. In the following, we will focus on recent Mueller-Navelet studies and we will also review the comparison with experimental data.

The initial idea behind considering the Mueller-Navelet jets cross section as a probe for BFKL physics is the following: in a hadron collider, let us assume that two partons interact (one from each hadron) such that in the final state we find a forward and backward jet of similar and sizeable p_T . Then these can be the hard scales attached to the two ends of a BFKL ladder and any collinear (DGLAP) logarithms are suppressed in the evolution from one jet to the other. The main contribution to this process on the partonic level then would come from the BFKL logarithms given that the two jets are well separated in rapidity. The process is depicted in Fig. 12.

One would think that already at Tevatron, the aim would be to see in the

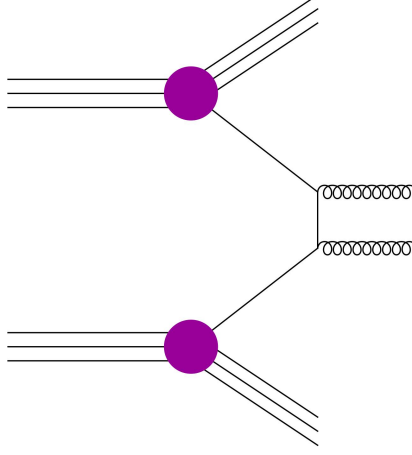


Figure 13. Diagrammatic tree level approximation for Mueller-Navelet jets.

data the power-like growth with energy of the cross section characteristic for BFKL dynamics. The problem with that though is that this growth is down due to the rapidly falling PDFs in forward-backward dijet production with large rapidity separation. For that reason, the main observable to be studied is the decorrelation in azimuthal angle between the two tagged jets as a function of the rapidity separation [44–47].

At tree level (Fig. 13), the produced jets have to be back-to-back due to energy-momentum conservation: the partonic cross section is a $2 \rightarrow 2$ process. As the partonic centre-of-mass energy increases though, the tree level approximation is not a good approximation at all. One is bound to consider extra real radiation in the final state which breaks the back-to-back configuration of the two outmost jets. The larger the available energy, the larger is the phase space and more emissions need to be considered in order to describe more accurately what really happens in the collider and the more azimuthally decorrelated is the system of the forward-backward jets. To measure the correlation, one projects the momenta of the two jets on the transverse plane and calculates the average $\cos(\Delta\phi)$, where $\Delta\phi$ is defined as the difference of the angles of the two jets minus π , $\Delta\phi = \phi_{J,1} - \phi_{J,2} - \pi$. One can go further along these lines and compute the following moments: $C_n = \langle \cos(n\Delta\phi) \rangle$, where n can be 1, 2 or 3. In an effort to minimise further any contamination from collinear logarithm, the ratios

$$\frac{C_n}{C_m} = \frac{\langle \cos(n\Delta\phi) \rangle}{\langle \cos(m\Delta\phi) \rangle} \quad (46)$$

have been proposed as better observables to probe BFKL dynamics [48–50].

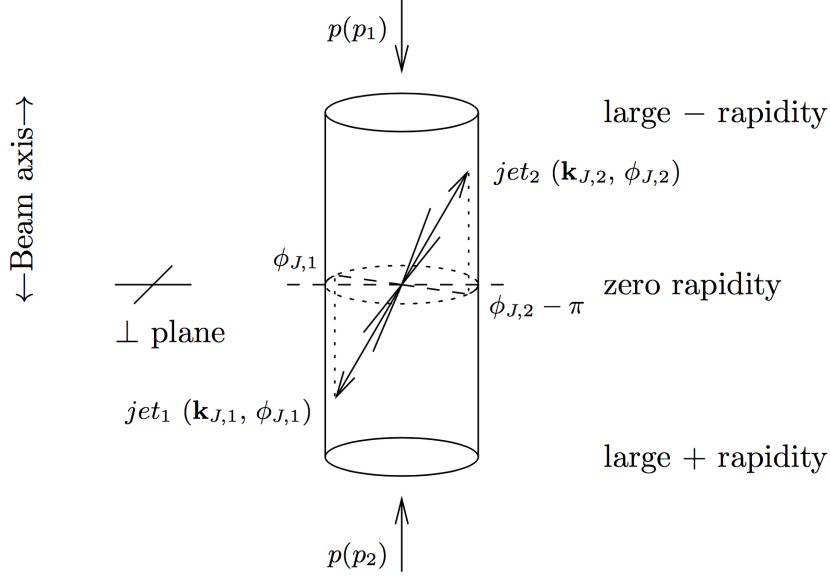


Figure 14. Tree level approximation for Mueller-Navelet jets in a collision setup. Figure taken from Ref. [52].

At the moment, we have two groups with full NLO BFKL predictions for Mueller-Navelet jet observables at LHC energies. Both groups are using an analytic approach (as opposed to Monte Carlo studies) [51–55]. In their studies, they compare and find good agreement with the average cosine ratios. This agreement was summarized in the results of CMS on multijet correlations [56] where Figs. 15 and 16 are taken from. The success of BFKL physics to describe the data for the average cosine ratios and the not so good performance of the standard collinear tools is a very promising starting point while waiting for relevant results from the second run of the LHC.

Recently, new observables sensitive to BFKL dynamics were proposed in the context of multijet production at the LHC [57, 58]. The idea is to study events with two tagged forward-backward jets, separated by a large rapidity span, and also tag on a third jet⁷ produced in the central region of rapidity, allowing for inclusive radiation in the remaining areas of the detectors. A kinematical configuration can be seen in Fig 17. The proposed distributions have a very different behavior to the ones characteristic of the Mueller-Navelet case. These new distributions are defined using the projec-

⁷ In Ref. [58], two –more central in rapidity– jets are tagged but we restrict the discussion here to the 3-jet observables.

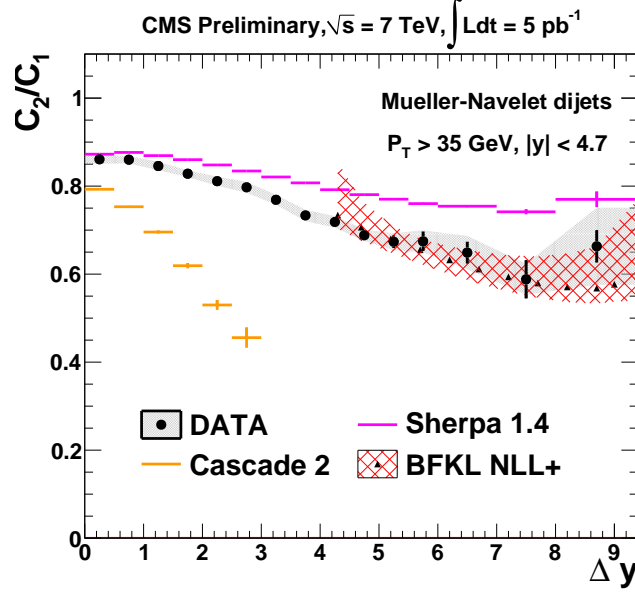


Figure 15. Ratio C_2/C_1 as a function of Δy compared to various theory predictions. Figure taken from Ref. [56].

tions on the two relative azimuthal angles formed by each of the forward jets with the central jet, $\Delta\phi_1 = \phi_1 - \phi_c - \pi$ and $\Delta\phi_2 = \phi_c - \phi_2 - \pi$. The experimentally relevant observable is the mean value in the selected events of the two cosines of the azimuthal angle differences, i.e. $\langle \cos(M\Delta\phi_1)\cos(N\Delta\phi_2) \rangle$. To eliminate again any collinear logarithm contamination, one can form ratios and finally the observables are defined as:

$$\mathcal{R}_{P,Q}^{M,N} = \frac{\langle \cos(M\Delta\phi_1)\cos(N\Delta\phi_2) \rangle}{\langle \cos(P\Delta\phi_1)\cos(Q\Delta\phi_2) \rangle}, \quad (47)$$

where M , N , P and Q can be equal to 1 or 2.

In Fig. 18 one sees plotted the ratio R_{22}^{12} after setting the momentum of the forward jet to $k_A = 40$ GeV, the momentum of the backward jet to $k_B = 50$ GeV and their rapidities to $Y_A = 10$ and $Y_B = 0$ respectively. For the transverse momentum of the central jet three values $k_J = 30, 45, 70$ GeV were chosen and the rapidity of the central jet y_J varies between the two rapidities of the forward-backward jets. The claim is that these ratio distributions as defined in Eq. 47 are probing the fine structure of the QCD radiation in the high energy limit and one should expect the LHC data to agree with the theoretical BFKL estimates especially in the regions where y_J is closer to $(Y_A - Y_B)/2$. Apart from the analytic approach followed in

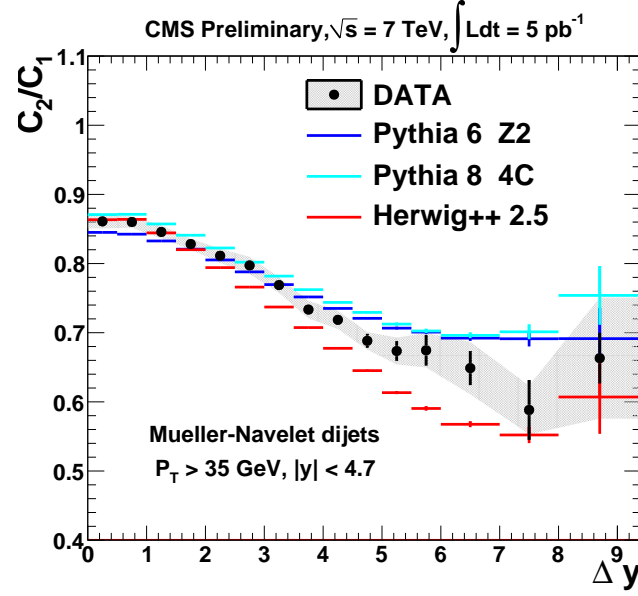


Figure 16. Ratio C_2/C_1 as a function of Δy compared to various theory predictions. Figure taken from Ref. [56].

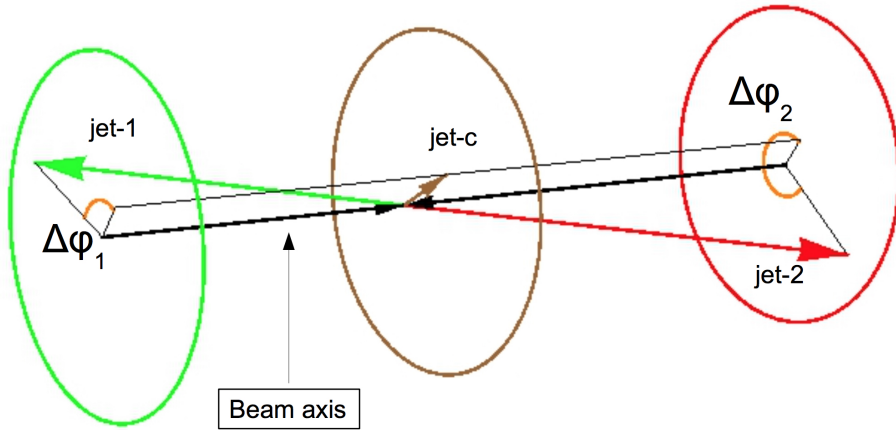


Figure 17. Kinematics of a 3-jet event.

Refs. [57, 58], it would be very important to compare against the BFKL Monte Carlo code BFKLex [59–66] for these proposed ratio observables.

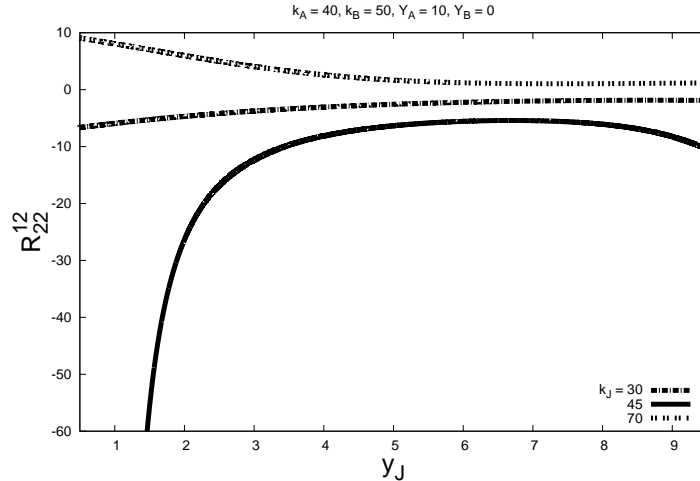


Figure 18. A study of the ratio R_{22}^{12} as defined in Eq. 47 for fixed values of the p_T of the two forward jets and three values of the p_T of the tagged central jet, as a function of the rapidity of the central jet y_J .

4. Discussion

The LHC has opened up a new era in particle physics. So far, there is no clear signal for new physics and the SM seems to secure even more its position as the best theory we have to describe the fundamental interactions (Gravity excluded). Despite that though, there is an awful lot we do not know about the SM. If we exclude lattice works, the only way we have at our disposal to do calculations is perturbation theory. And clearly, knowing the first two-three terms of an expansion to a function does not give a full insight to the function itself and its special properties. It only allows to learn about the behavior of the function in the small region where the expansion makes sense. It remains to be seen whether the LHC era will be an exciting time of new physics but even if not, it should be the era in which we learn and understand more about the SM, especially more so if it surfaces at the end of the day as the only fundamental theory available to describe consistently experimental data.

To that end, the role of phenomenology is crucial. We do not calculate theoretical estimates and then compare to data sets in order to fill out a checklist of processes. We do confront our theory using the experiment because we want to understand better our theory. We want to see

whether different approaches within the same fundamental model can reveal properties that were previously masked. Phenomenology in modern particle physics, apart from carrying the responsibility of validating or falsifying a theory, it should also shed light to corners of a valid theory that are not in plain view.

BFKL physics is connected to some very important and still open issues within QCD and beyond. Factorization theorems, the transition from the perturbative to the non-perturbative regime, the correct degrees of freedom in high energies, the connection of QCD to the old Regge theory are few examples. BFKL phenomenology should try to give answers to all these important questions. Before that though, it needs to answer the most pressing question: which is the rough collision energy threshold after which BFKL dynamics becomes—for the relevant kinematical configurations—, if not dominant, at least the main player. Does the LHC reach beyond that threshold? In that respect, to find the window of applicability for this formalism, more work is needed in identifying observables where the BFKL approach is distinct. We should define more exclusive experimental quantities such that BFKL fits the measured data and all other possible approaches fail if we are already beyond the threshold at the LHC. It remains to be seen whether the second run of the LHC will be the time of great progress for BFKL phenomenology.

Acknowledgements

The author would like to thank the organisers and in particular C. Royon for the invitation, all the help and the warm hospitality.

References

- [1] L. N. Lipatov, Sov. J. Nucl. Phys. **23**, 338 (1976) [Yad. Fiz. **23**, 642 (1976)].
- [2] V. S. Fadin, E. A. Kuraev and L. N. Lipatov, Phys. Lett. B **60**, 50 (1975).
- [3] E. A. Kuraev, L. N. Lipatov and V. S. Fadin, Sov. Phys. JETP **44**, 443 (1976) [Zh. Eksp. Teor. Fiz. **71**, 840 (1976)].
- [4] I. I. Balitsky and L. N. Lipatov, Sov. J. Nucl. Phys. **28**, 822 (1978) [Yad. Fiz. **28**, 1597 (1978)].
- [5] V. S. Fadin and L. N. Lipatov, Phys. Lett. B **429**, 127 (1998) [hep-ph/9802290].
- [6] M. Ciafaloni and G. Camici, Phys. Lett. B **430**, 349 (1998) [hep-ph/9803389].
- [7] V. Barone and E. Predazzi, *High-Energy Particle Diffraction*, Springer 2002.
- [8] J. R. Forshaw and D. A. Ross, *Quantum Chromodynamics and the Pomeron*, Cambridge 1997 (Cambridge lecture notes in physics 9).

- [9] B. L. Ioffe, V. S. Fadin and L. N. Lipatov, *Quantum Chromodynamics. Perturbative and Nonperturbative Aspects*, Cambridge 2014 (Cambridge Monographs on Particle Physics, Nuclear Physics and Cosmology 30).
- [10] V. Del Duca, hep-ph/9503226.
- [11] G. P. Salam, Acta Phys. Polon. B **30**, 3679 (1999) [hep-ph/9910492].
- [12] V. S. Fadin, hep-ph/9807528.
- [13] V. S. Fadin, R. Fiore, M. I. Kotsky and A. Papa, Phys. Rev. D **61**, 094006 (2000) [hep-ph/9908265].
- [14] M. Ciafaloni and G. Rodrigo, JHEP **0005**, 042 (2000) [hep-ph/0004033].
- [15] V. S. Fadin, R. Fiore, M. I. Kotsky and A. Papa, Phys. Rev. D **61**, 094005 (2000) [hep-ph/9908264].
- [16] D. Y. Ivanov, M. I. Kotsky and A. Papa, Eur. Phys. J. C **38**, 195 (2004) [hep-ph/0405297].
- [17] D. Y. Ivanov, M. I. Kotsky and A. Papa, Nucl. Phys. Proc. Suppl. **146**, 117 (2005).
- [18] J. Bartels, D. Colferai and G. P. Vacca, Eur. Phys. J. C **29**, 235 (2003) [hep-ph/0206290].
- [19] J. Bartels, D. Colferai and G. P. Vacca, Eur. Phys. J. C **24**, 83 (2002) [hep-ph/0112283].
- [20] F. Caporale, D. Y. Ivanov, B. Murdaca, A. Papa and A. Perri, JHEP **1202**, 101 (2012) [arXiv:1112.3752 [hep-ph]].
- [21] D. Y. Ivanov and A. Papa, JHEP **1205**, 086 (2012) [arXiv:1202.1082 [hep-ph]].
- [22] D. Y. Ivanov and A. Papa, JHEP **1207**, 045 (2012) [arXiv:1205.6068 [hep-ph]].
- [23] G. Chachamis, M. Hentschinski, J. D. Madrigal Martinez and A. S. Vera, Phys. Rev. D **87**, no. 7, 076009 (2013) [arXiv:1212.4992].
- [24] G. Chachamis, M. Hentschinski, J. D. Madrigal Martinez and A. Sabio Vera, Phys. Part. Nucl. **45**, no. 4, 788 (2014) [arXiv:1211.2050 [hep-ph]].
- [25] J. Bartels, D. Colferai, S. Gieseke and A. Kyrieleis, Phys. Rev. D **66**, 094017 (2002) [hep-ph/0208130].
- [26] J. Bartels and A. Kyrieleis, Phys. Rev. D **70**, 114003 (2004) [hep-ph/0407051].
- [27] J. Bartels, S. Gieseke and C. F. Qiao, Phys. Rev. D **63**, 056014 (2001) [Phys. Rev. D **65**, 079902 (2002)] [hep-ph/0009102].
- [28] J. Bartels, S. Gieseke and A. Kyrieleis, Phys. Rev. D **65**, 014006 (2002) [hep-ph/0107152].
- [29] G. Chachamis and J. Bartels, PoS DIFF **2006**, 026 (2006).
- [30] I. Balitsky and G. A. Chirilli, Phys. Rev. D **87**, no. 1, 014013 (2013) [arXiv:1207.3844 [hep-ph]].
- [31] I. Balitsky and G. A. Chirilli, Phys. Rev. D **83**, 031502 (2011) [arXiv:1009.4729 [hep-ph]].
- [32] G. Chachamis, M. Deak and G. Rodrigo, PoS EPS **-HEP2013**, 092 (2013) [arXiv:1310.7763 [hep-ph]].
- [33] G. Chachamis, M. Deak and G. Rodrigo, PoS DIS **2014**, 085 (2014).

- [34] G. Chachamis, M. Deak and G. Rodrigo, JHEP **1312**, 066 (2013) [arXiv:1310.6611 [hep-ph]].
- [35] V. S. Fadin, Zh. Eksp. Teor. Fiz. Pis'ma **61** (1995) 342; V. S. Fadin, R. Fiore and A. Quartarolo, Phys. Rev. **D53** (1996) 2729; V. S. Fadin, M. I. Kotsky, Yad. Fiz. **59**(6) (1996) 1; V. S. Fadin, M. I. Kotsky and R. Fiore, Phys. Lett. **B359** (1995) 181.
- [36] V. S. Fadin and L. N. Lipatov, Nucl. Phys. **B406** (1993) 259; V. S. Fadin, R. Fiore and A. Quartarolo, Phys. Rev. **D50** (1994) 5893
- [37] V. S. Fadin, M. I. Kotsky and L. N. Lipatov, Phys. Lett. **B415** (1997) 97.
- [38] S. Catani, M. Ciafaloni and F. Hautmann, Phys. Lett. **B242** (1990) 97; Nucl. Phys. **B366** (1991) 135; G. Camici and M. Ciafaloni, Phys. Lett. **B386** (1996) 341; V. S. Fadin, R. Fiore, A. Flachi and M. I. Kotsky, Phys. Lett. **B422** (1998) 287
- [39] M. Ciafaloni, D. Colferai and G. P. Salam, Phys. Rev. **D60** (1999) 114036
- [40] Y. L. Dokshitzer, Sov. Phys. JETP **46**, 641 (1977) [Zh. Eksp. Teor. Fiz. **73**, 1216 (1977)].
- [41] V. N. Gribov and L. N. Lipatov, Sov. J. Nucl. Phys. **15**, 438 (1972) [Yad. Fiz. **15**, 781 (1972)].
- [42] G. Altarelli and G. Parisi, Nucl. Phys. B **126**, 298 (1977).
- [43] A. H. Mueller and H. Navelet, Nucl. Phys. B **282** (1987) 727.
- [44] V. Del Duca and C. R. Schmidt, Phys. Rev. D **49** (1994) 4510 [hep-ph/9311290].
- [45] W. J. Stirling, Nucl. Phys. B **423** (1994) 56 [hep-ph/9401266].
- [46] L. H. Orr and W. J. Stirling, Phys. Rev. D **56** (1997) 5875 [hep-ph/9706529].
- [47] J. Kwiecinski, A. D. Martin, L. Motyka and J. Outhwaite, Phys. Lett. B **514** (2001) 355 [hep-ph/0105039].
- [48] A. Sabio Vera, Nucl. Phys. B **746** (2006) 1 [hep-ph/0602250].
- [49] A. Sabio Vera and F. Schwennsen, Nucl. Phys. B **776** (2007) 170 [hep-ph/0702158 [HEP-PH]].
- [50] M. Angioni, G. Chachamis, J. D. Madrigal and A. Sabio Vera, Phys. Rev. Lett. **107**, 191601 (2011) doi:10.1103/PhysRevLett.107.191601 [arXiv:1106.6172 [hep-th]].
- [51] B. Ducloue, L. Szymanowski and S. Wallon, JHEP **1305**, 096 (2013) [arXiv:1302.7012 [hep-ph]].
- [52] D. Colferai, F. Schwennsen, L. Szymanowski and S. Wallon, JHEP **1012**, 026 (2010) [arXiv:1002.1365 [hep-ph]].
- [53] B. Ducloue, L. Szymanowski and S. Wallon, Phys. Rev. Lett. **112**, 082003 (2014) [arXiv:1309.3229 [hep-ph]].
- [54] F. Caporale, D. Y. Ivanov, B. Murdaca and A. Papa, Eur. Phys. J. C **74**, 3084 (2014) [arXiv:1407.8431 [hep-ph]].
- [55] F. G. Celiberto, D. Y. Ivanov, B. Murdaca and A. Papa, Eur. Phys. J. C **75**, no. 6, 292 (2015) doi:10.1140/epjc/s10052-015-3522-6 [arXiv:1504.08233 [hep-ph]].

- [56] G. Safronov [CMS Collaboration], AIP Conf. Proc. **1654**, 040003 (2015) [arXiv:1501.02332 [hep-ex]].
- [57] F. Caporale, G. Chachamis, B. Murdaca and A. Sabio Vera, arXiv:1508.07711 [hep-ph].
- [58] F. Caporale, F. G. Celiberto, G. Chachamis and A. Sabio Vera, arXiv:1512.03364 [hep-ph].
- [59] G. Chachamis and A. Sabio Vera, PoS DIS **2013** (2013) 167 [arXiv:1307.7750].
- [60] F. Caporale, G. Chachamis, J. D. Madrigal, B. Murdaca and A. Sabio Vera, Phys. Lett. B **724** (2013) 127 [arXiv:1305.1474 [hep-th]].
- [61] G. Chachamis, A. Sabio Vera and C. Salas, Phys. Rev. D **87** (2013) 1, 016007 [arXiv:1211.6332 [hep-ph]].
- [62] G. Chachamis and A. Sabio Vera, Phys. Lett. B **717** (2012) 458 [arXiv:1206.3140 [hep-th]].
- [63] G. Chachamis and A. Sabio Vera, Phys. Lett. B **709** (2012) 301 [arXiv:1112.4162 [hep-th]].
- [64] G. Chachamis, M. Deak, A. Sabio Vera and P. Stephens, Nucl. Phys. B **849** (2011) 28 [arXiv:1102.1890 [hep-ph]].
- [65] G. Chachamis and A. Sabio Vera, arXiv:1511.03548 [hep-ph].
- [66] G. Chachamis and A. Sabio Vera, arXiv:1512.03603 [hep-ph].